Received: 2 February 2024 | Revised: 5 June 2024 | Accepted: 20 June 2024

IET Generation, Transmission & Distribution

DOI: 10.1049/gtd2.13214

The Institution of Engineering and Technology WILEY

ORIGINAL RESEARCH

Preventive DC-side decoupling: A system integrity protection scheme to limit the impact of DC faults in offshore multi-terminal HVDC systems

Patrick Düllmann[1] | **Christopher Klein**[1] | **Pascal Winter**[2] | **Hendrik Köhler**[2] | **Michael Steglich**[2] | **Jan Teuwsen**[2] | **Willem Leterme**[1]

[1]Institute for High Voltage Equipment and Grids, Digitalization and Energy Economics (IAEW), Faculty of Electrical Engineering and Information Technology, RWTH Aachen University, Aachen, Germany

[2]Offshore, Amprion GmbH, Dortmund, Germany

Correspondence
Patrick Düllmann, Institute for High Voltage Equipment and Grids, Digitalization and Energy Economics (IAEW), Faculty of Electrical Engineering and Information Technology, RWTH Aachen University, Schinkelstrasse 2, Aachen, Germany.
Email: p.duellmann@iaew.rwth-aachen.de

Abstract

To create synergies between offshore wind integration and operational flexibility, interconnecting HVDC links to multi-terminal networks is highly desired. However, its technical realisation remains a major challenge: In particular, it is crucial to prevent DC faults from leading to an intolerable loss of power infeed to the connected AC grids. To restrict this loss of power infeed, this paper proposes a concept for linear HVDC networks that is based on state-of-the-art equipment only—that is, without dependence on DC circuit breakers. In this concept, the DC interconnection is preventively decoupled via DC high-speed switches whenever the cumulative wind infeed exceeds the frequency containment reserve of the AC grid, but remains coupled at all other times. The decoupling is realised via controlling the coupling line current to zero through coordinated setpoint changes for the converters' (V_{DC}/P)-droop controls. Both the decoupling sequence and the DC fault behaviour in decoupled state are validated via EMT simulations. In addition, limitations with regard to expandability are discussed. The proposed concept may not only limit the loss of infeed, but mitigates risks as a fall-back level for more complex offshore (multi-vendor) multi-terminal HVDC topologies—and may thus accelerate their development at reasonable costs.

1 | INTRODUCTION

For the integration of offshore wind farms (OWF), point-to-point HVDC links in symmetric monopole configuration are considered the state of the art. To cope with the massive increase of large-scale offshore wind power that is foreseen for the upcoming decades, the next generation of European offshore HVDC links will be realised in a bipolar configuration with dedicated metallic return (DMR) at a standardised 2 GW rating (Figure 1) [1]. Additionally, it is envisioned to plan those bipole systems ready for future DC interconnections [2–4]. These interconnections to a multi-terminal DC (MTDC) configuration could lift operational and economic benefits, but at the same time come with several technical challenges [5]. While different MTDC topologies (radial, linear, ring, meshed) up to an offshore HVDC grid [6, 7] are discussed for the future, connecting two point-to-point links at the offshore stations via a DC line—resulting in a Π-shape, so-called "linear" topology—is one of the simplest options (Figure 1) [8, 9].

As this multi-terminal topology is comparatively simple, and may increase both redundancy and operational flexibility via just adding a short additional cable, it can be a first step providing a viable path to larger HVDC grid structures. It allows the interconnection of offshore platforms at times when the specification of large offshore grids is not yet feasible due to ongoing technological developments. This way, it can generate valuable risk-mitigating experience in terms of planning and operation of multi-terminal HVDC systems. In order to achieve a positive net value of the investment in a linear DC-side interconnection, the system's control and protection needs to be adaptable with

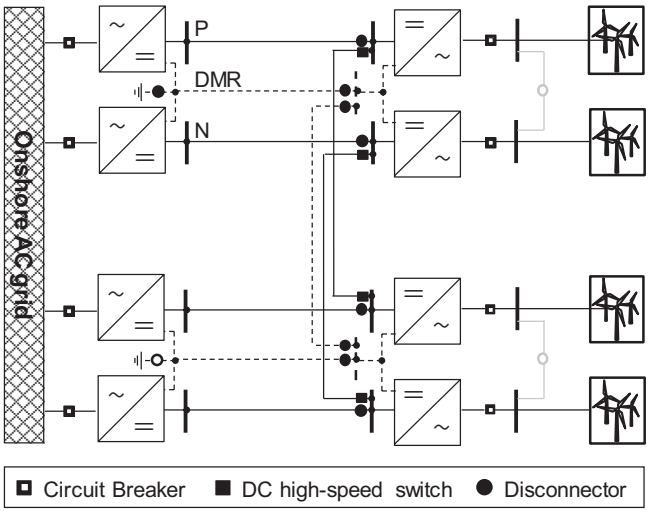

FIGURE 1 Π-configuration overview—DC-side connection of two offshore HVDC links in bipole configuration with dedicated metallic return (DMR) [14].

sufficiently low additional costs. However, this is considered especially challenging for the DC protection: With an interconnection, the cumulative power of the system can exceed the frequency containment reserve (FCR) of the onshore AC grid. Thus, a core constraint for the protection is to limit the fault-induced maximum power loss to values below the FCR limit with reasonable risk and effort; this applies already to the aforementioned small, linear, Π-shaped MTDC systems.

Several different protection concepts for MTDC systems have been studied in research and development [10]. Typically, their limitation of the DC fault's impact relies on a varying number of direct current circuit breakers (DCCBs) combined with large inductors. However, MTDC protection systems based on DCCBs have not yet been implemented in Europe, resulting in a lack of experience and confidence. As standards for HVDC interoperability are still missing, there is a risk to encounter undesired or unexpected system behaviour in (multi-vendor) multi-terminal setups. In [11], ENTSO-E describes a "vicious cycle" in the current development stage: Without operational experience, TSOs might not be fully able to specify technical requirements for control and protection in (multi-vendor) MTDC systems, such that manufacturers might not be able to develop products that match such specifications and that are interoperable. Further, DCCB-based solutions come with higher additional investment costs—possibly not only related to the DCCB itself, but also related to other system adaptions (e.g. the DC-FRT capabilities of converters [12]).

To address both abovementioned challenges, an operational system integrity protection scheme (SIPS, cf. [13]) for small-scale linear MTDC systems—as first proposed in [14]—is further developed and discussed in this paper. The concept is developed as an option to realise first offshore multi-terminal HVDC networks without the need to specify and realise DCCB-based protection systems, while still limiting the power loss seen at the onshore AC side in case of DC faults. Compared to DCCB-based protection systems–for which interoperability issues may increase the risk of DCCB failures or undesired converter blocking despite DCCB operation, and thus the risk of exceeding the tolerable power loss—preventive decoupling is expected to have lower risks. In particular, with the preventive decoupling concept, the "vicious cycle" in designing first MTDC systems is split into smaller parts: Potentially, control and protection requirements could be specified mutually independent. However, the decoupling concept comes with operational restrictions, and its expandability to larger structures or HVDC grids is limited.

In Section 2, the investigation framework is introduced, and the concept is compared to DCCB-based MTDC protection on a conceptual level. Subsequently, the EMT simulation study and the chosen implementation of the decoupling sequence are outlined in Section 3. To validate the concept, simulation results are presented in Section 4, and remaining challenges are discussed—including the re-coupling. Section 5 deals with the expandability to larger MTDC networks, before Section 6 concludes the paper by summarising key findings.

2 | CONCEPTUAL ANALYSIS: MTDC FAULT BEHAVIOUR

2.1 | Investigation framework: Offshore interconnection

According to specific plans for HVDC system development towards 2030, a trend towards 2 GW systems in bipolar configuration with DMR and with a rated DC voltage of 525 kV can be observed [1]. In these systems, it is expected that state-of-the-art Modular Multilevel Converters (MMCs) with half-bridge submodules are used as converter technology. With regard to the cable-based transmission systems, there are two possible realisations: P, DMR, and N cables separately trenched, or all three cables buried as a bundle [9, 15]. On the offshore wind farm side, a 66 kV direct connection is the current standard in Germany—while higher voltages (e.g., 132 kV) are being discussed for future systems. In their normal operation, the wind farms connected to the P and N pole converters of the bipolar HVDC system are assumed to be operated in a decoupled manner.

A linear DC-side interconnection of such bipolar point-to-point links as a prospective system topology for first offshore multi-terminal HVDC networks in Europe is shown in Figure 1 [14]. Whereas for the two independent bipolar point-to-point links, the outage of 2 GW in case of a pole-pole-ground fault—which is a realistic scenario if P, N, and DMR cables are bundled [15]—can be tolerated, this is not the case anymore for the linear multi-terminal connection. Since the onshore stations are connected to the same synchronous AC transmission network, the temporary power loss caused by a single DC fault could reach the size of the entire MTDC system's rating (here: 4 GW). This is the case when: (a) no additional protection measures are taken (i.e. when a non-selective concept as defined in [10] is chosen) or (b) when there is a protection failure in a partially

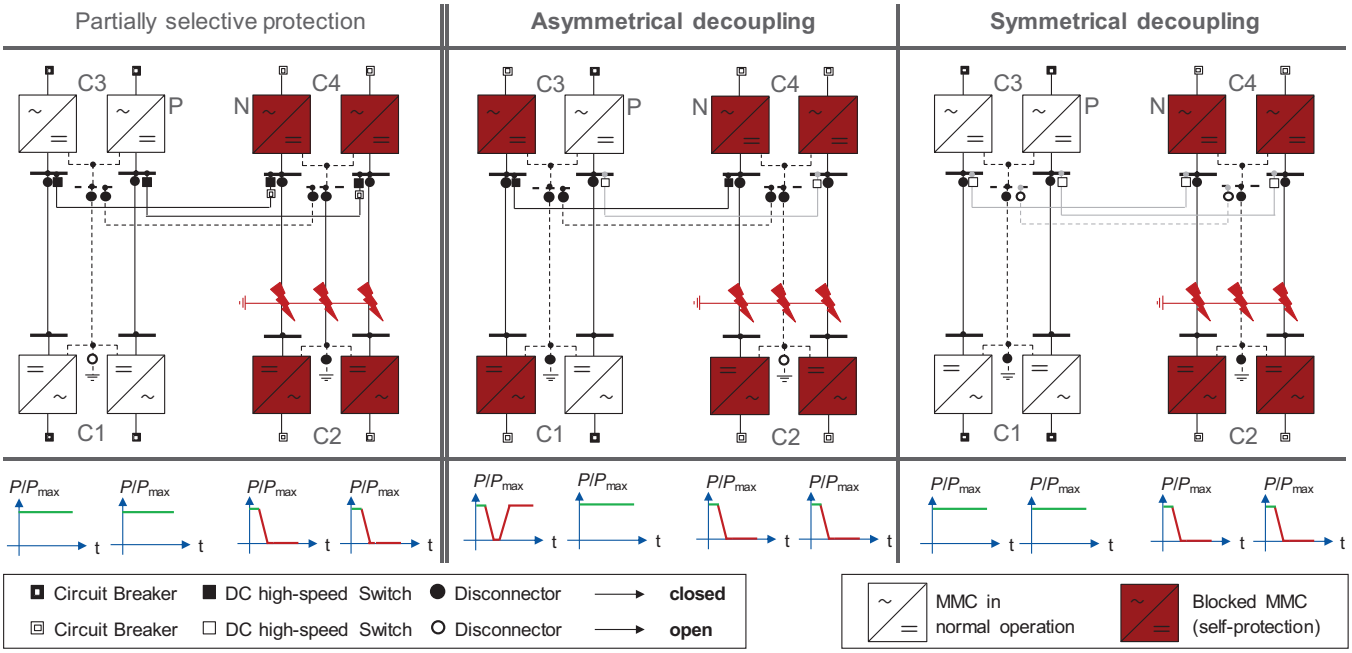

FIGURE 2 Use of DC circuit breakers (DCCBs) for partially selective protection versus preventive decoupling strategies (symmetrical/asymmetrical). Prospective converter reactions and time-dependent power loss (qualitative) following a pole-pole-ground cable fault [14].

or fully selective protection setup (e.g. DCCB not opening). However, when connecting to the Continental European (CE) grid, the reference incident is defined as a loss of 3 GW [16, 17]—and is even smaller for other synchronous grid areas. Although higher temporary outages might be permissible in the future (cf. [18, 19]), this reference incident—albeit dimensioned for permanent outages—is the only binding guideline that exists at the moment, and is therefore considered in this paper.

Therefore, to limit the temporary loss of power infeed in case of DC faults to a maximum of 3 GW, operational strategies and/or dedicated DC protection systems are required.

2.2 | Review: Options for DC fault protection

To protect the considered 4-GW system, partially or fully selective strategies as defined in [10] might be options to keep the power loss below acceptable limits [8]. In Figure 2 (left), a partially selective approach employing two DCCBs is shown for comparison, as it could be sufficient to limit the power loss to values of 2 GW—that is, to the maximum power loss resulting with two independent point-to-point links [8]. However, for the realisation of this protection concept, fast DCCBs—which lack any operational experience in Europe—and large inductors are required. These DCCBs and inductances are costly and require large additional spaces on offshore platforms. Furthermore, to achieve the desired protection performance, the design of the protection system's devices (DCCBs, fault current limiting reactors, relays, etc.) has to be specified, and needs to be coordinated with the control and protection of all converters [12, 20]. Otherwise, converters in the non-affected protection zone might still be blocked for self-protection, resulting in an intolerable temporary power loss of up to 4 GW [21, 22].

Ensuring the required coordination and interoperability between all protection-related components is challenging—already in single-vendor setup, but especially in a multi-vendor system with DC-side grid codes not yet available [11, 20]. Additionally, several aspects not related to protection are equally challenging and deserve attention, for example, control stability during normal operation and dynamic events [11]. Therefore, the option to realise a first MTDC network without the use of a dedicated DCCB-based protection system could be an option to reduce the complexity of interdependencies between control and protection. The focus of the specification and development could be on control interoperability challenges, and first operational experience could be gained. However, a practical strategy is needed to reliably limit the DC fault-induced loss of power infeed to 3 GW in the absence of a DCCB-based protection system.

While also other proposed DC protection strategies, for example, non-selective protection based on fault-blocking MMCs (cf. [23]), do work without DCCBs, they a) require a different converter technology, b) come with additional challenges of control/protection coordination, and c) exceed the power loss of 3 GW per definition—albeit just temporarily.

2.3 | Proposal: Preventive decoupling strategy

To address the issue of power loss limitation in case of DC faults while (partly) decoupling the interoperability

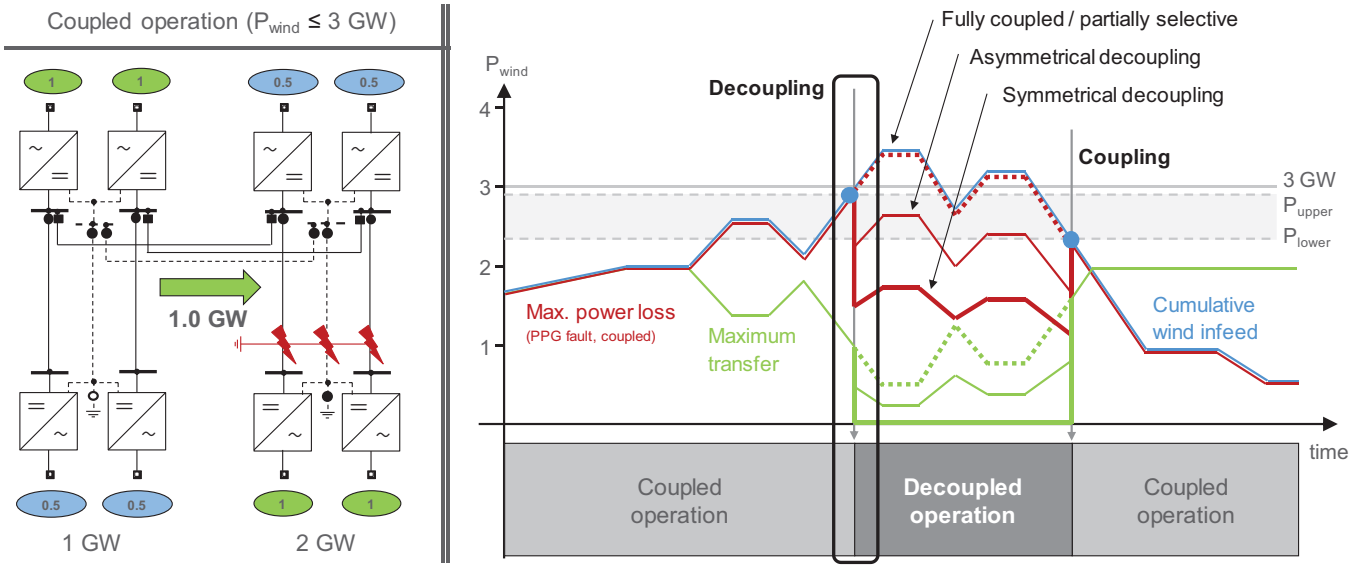

FIGURE 3 Explanation of the preventive decoupling concept via an example timeline of cumulative wind infeed (blue), and the resulting timelines of (a) sum of onshore power loss in case of a pole-pole-ground (P-P-G) fault (red), and (b) maximum possible power transfer via the coupling line (green). Shown for "partially selective / coupled" vs. "symmetrical decoupling" versus "asymmetrical decoupling".

challenges regarding control and protection for first offshore multi-terminal HVDC networks, the operational strategy of "preventive decoupling" is introduced in this paper. As shown in Figures 2 (middle, right)–5, preventive decoupling describes the intentional, temporary disconnection of the offshore DC interconnection cable between the two interconnected HVDC export links via opening DC high-speed switches (DC-HSS)—or DC disconnectors, whose disadvantages are discussed in Section 4.3—at both line ends during normal operation. Two decoupling concepts are distinguished [14]:

a. Asymmetrically (Figure 2 middle): Opening of DC-HSS only on one pole, still operating the system as one network after the decoupling action, or
b. Symmetrically (Figure 2 right): Opening DC-HSSs on both poles, identical to two independent point-to-point systems after the decoupling action.

The concept is rather an operational concept or system integrity protection scheme (SIPS), so a preventive protection action instead of a curative protection reaction to a fault, and is visualised in Figures 3 and 4. In situations where the total wind power infeed is sufficiently lower than 3 GW, the system is operated fully coupled as a non-selectively protected multi-terminal network (cf. Figure 3, "coupled operation"): All DC-HSSs are closed, and DC faults are cleared via converter blocking and subsequent opening of AC circuit breakers (ACCBs) at all four stations. In case of a pole-pole-ground fault, the maximum temporary power loss is equal to the total amount of wind power infeed (cf. Figure 3) [14].

As soon as the wind forecast (and/or the measurement, or another criterion to be chosen by a system operator) indicates a cumulative infeed of 3 GW or higher, the strategy of preventive decoupling is to initiate an operationally scheduled decoupling sequence via a secondary control/master control as indicated in Figure 6. This sequence changes the system topology to one of the topologies depicted in Figure 2 (middle, right) by opening the DC-HSS during the normal operation of the system. Once the decoupling sequence is completed and the system reached the intended decoupled state, the wind power infeed can be controlled to values above 3 GW. Then, even in cases where the wind infeed exceeds 3 GW, the maximum fault-induced loss of power infeed is limited without the use of DCCBs—either to <3 GW (asymmetrical decoupling), or to <2 GW (symmetrical decoupling, comparable to a partially selective protection setup), as indicated in Figures 2 and 3 [14].

The system will remain in this decoupled operation until the wind infeed is forecasted to fall below 3 GW for a significant period of time. In this case, the topology can be changed back via a coupling sequence, and subsequently the system is operated fully coupled again. For the initiation of the coupling sequence, different criteria could be used. For example, a hysteresis (between P_{upper} and P_{lower}) would be an option to avoid changing the topology too often and thereby reduce tear and wear of the DC high-speed switches. An example realisation of the SIPS logic inside a master controller is shown as a flow chart/state chart in Figure 4, where also necessary inputs and outputs that need to be accessible for the logic are highlighted. Another option could be to decide based on operational criteria—that is based on grid simulations that determine the necessity of a coupled operation for the predicted duration of a wind infeed below 3 GW.

As visible from Figure 3 (in particular the curve "maximum transfer"), the decoupling not only influences the fault behaviour, but also—contrary to the use of DCCBs, which only open in the event of a fault—the behaviour and flexibility

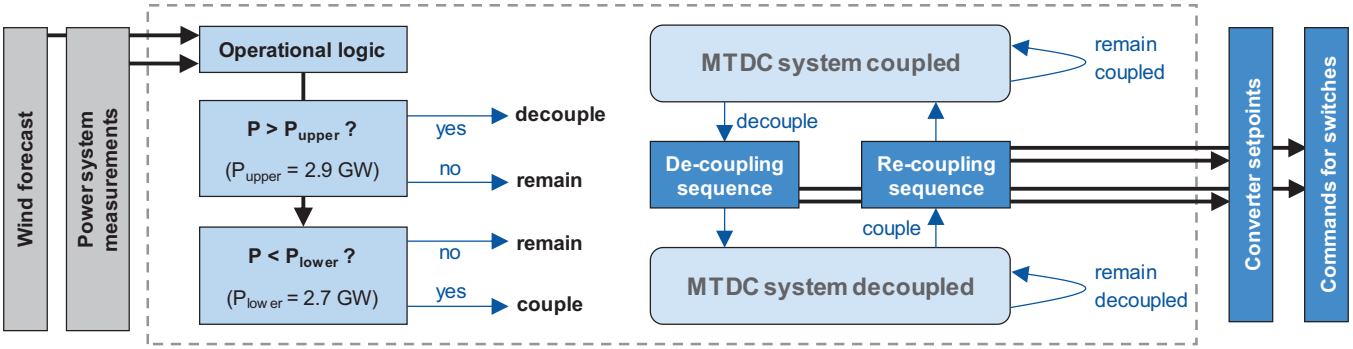

FIGURE 4 Flow chart for operational protection scheme: Inputs, logic overview, and outputs—example values for P_{upper}/P_{lower} (MTDC = Multi-Terminal DC)

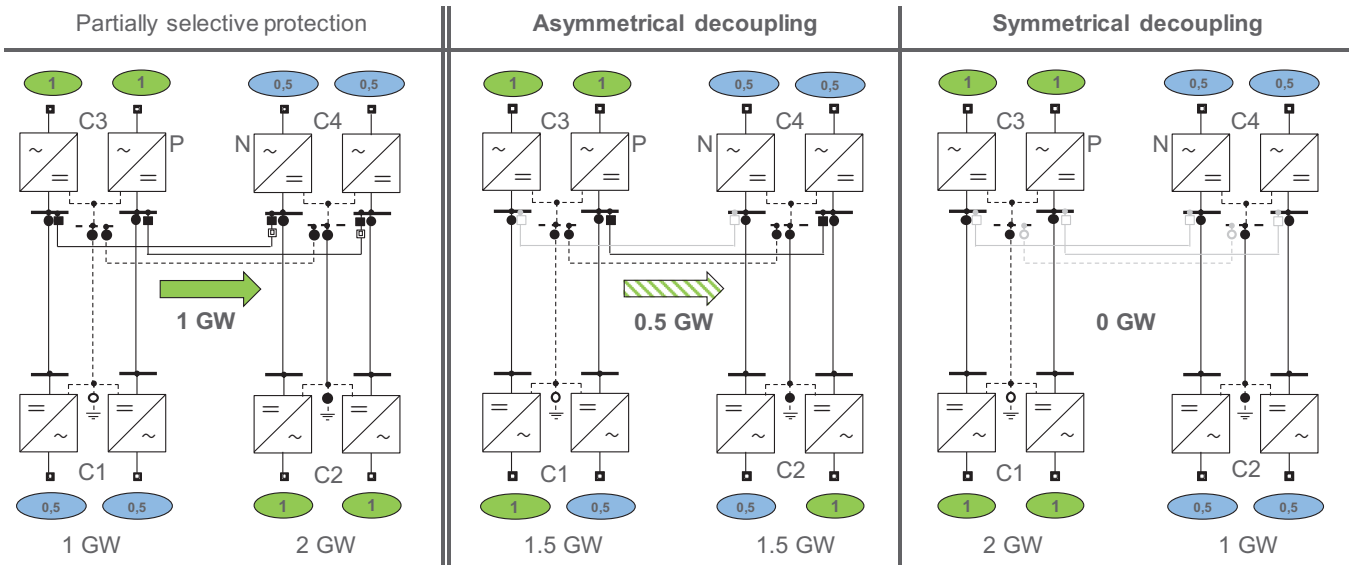

FIGURE 5 Use of DCCBs for partially selective protection vs. preventive decoupling strategies: Limitation in power transmission via offshore coupling cable during normal operation—here, wind infeed of 3 GW with maximum difference between C3 and C4 [14].

during normal operation. Figure 5 shows the worst case operational restrictions in power transfer for both decoupling options (Figure 5, middle, right), and compares these restrictions to the power flow in fully coupled operation (Figure 5, left)—which would be possible only with a dedicated DC-side protection concept, for example, with partially selective protection. For an example scenario of boundary wind infeed (cumulative wind infeed is 3 GW, unequal distribution), it is shown that the decoupled operation limits the maximum transferable power: From 1 GW (fully coupled), via 0.5 GW (asymmetrically decoupled), to 0 GW (symmetrically decoupled). This must be considered a significant limitation of the operational flexibility—which is one of the main benefits of multi-terminal HVDC networks.

When weighing up this drawback against the aforementioned benefits, it should be considered that a wind infeed of >75% (equal to >3 GW) only occurs in 2500 hrs/year—assuming that the wind farm outputs are fully correlated [24]; thus, the system will be operated in a coupled manner for the majority of time. Furthermore, the power transferable via the coupling link (coupled state, green curve in Figure 3) decreases with increasing wind power infeed, as the unused capacity of the export links is decreasing. The case depicted in Figure 3 (left) and Figure 5 already is the worst case. For full wind power infeed (4 GW), the maximum transfer is 0 GW either way [14].

To fully assess the impact of the preventive decoupling strategy on grid operation, and to quantify the reduced benefits of an MTDC system with decoupling strategy compared to an MTDC system that is always interconnected, more detailed studies (e.g., market simulation, load flow calculation, redispatch simulation) would be required, but are out of scope of this paper. Finally, the restriction of benefits has to be weighed against the costs and risks of alternative solutions that would allow a full coupling at all times—that is, DCCB-based protection (e.g. Figure 5 left).

Overall, to the authors of this paper, preventive DC-side decoupling appears to be a reasonable approach to interconnect offshore HVDC systems feeding the same synchronous grid area. From an AC stability perspective, this DC-side decoupling strategy may enable the usage of MTDC system advantages (e.g.,

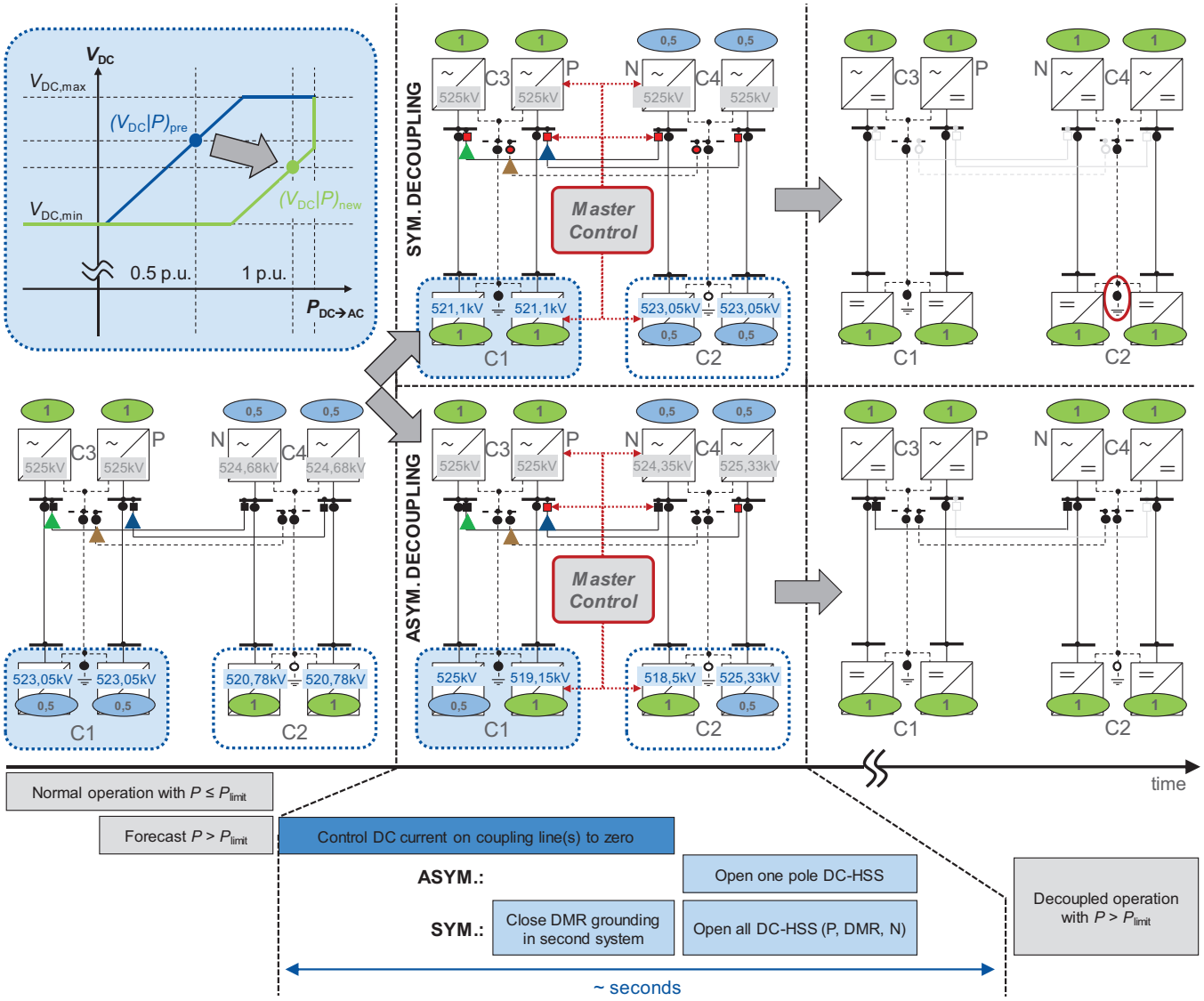

FIGURE 6 Decoupling sequence; top: symmetrical; bottom: asymmetrical; converters marked with blue dotted line: droop setpoint change for zero current control required; dotted lines filled in light blue: example setpoint change shown at top left [14]. (HSS = High-Speed Switch)

redundancy, reduction of redispatch, power flow control) in all network situations except for those with a high wind infeed, but at the same time limits threats to AC system stability when severe DC-side faults occur. Still, the concept has limitations and challenges, which are discussed in Section 4.3 and—with regard to expansions—in Section 5.

3 | PREVENTIVE DECOUPLING: SIMULATION STUDY

In the following, the exact procedures and realisations for symmetrical and asymmetrical preventive DC-side decoupling are discussed. The focus of the conducted simulation study is on the decoupling sequences—that is, the overall control concept, the mathematical setpoint calculation for symmetrical and asymmetrical operation of bipolar MTDC networks, and the sequence of DC-HSS operation.

3.1 | EMT modelling

To investigate the proposed preventive decoupling strategy for the system topology shown in Figure 1, an EMT simulation model similar to that used in [8] is applied and adapted [14]. Electrical converter models (type-4, parameters see Table 1), converter controls, wind farm models (aggregated), and frequency-dependent cable and DC fault models are described in [8] in more detail. The cable length is assumed to 300 km for both export links, and 50 km for the interconnection. The specific resistance per unit length of the cables that is implemented in the frequency-dependent models is set to

TABLE 1 Ratings for converters, DC network and AC grid—system ratings oriented at [1] and [8], MMC ratings at [2].

Symbol	Parameter	Rating
S	Rated power (per pole)	1054 MVA
P	Rated active power (per pole)	1000 MW
$V_{ac,grid}$	Rated AC voltage (grid, $f = 50$ Hz)	400 kV
$V_{ac,OWP}$[a]	Rated AC voltage (OWP, $f = 50$ Hz)	66 kV
V_{ac}	Rated AC voltage (secondary side)	300 kV (RMS, L-L)
V_{dc}	Rated DC voltage	±525 kV
N_{SM}	Number of SM/arm	215
V_{SM}[b]	Rated submodule voltage	2.7 kV
C_{SM}	Submodule capacitance	9.0 mF (≈40 kJ/MVA)
$I_{arm,RMS}$	Rated arm current (RMS)	1.20 kA
$I_{arm,peak}$	Rated arm current (peak)	2.07 kA
$I_{C,RM}$	IGBT repetitive peak current	4.0 kA
L_{arm}	Arm inductors	50 mH
$L_{dc,term}$	DC terminal inductor	25 mH

[a]OWP = Offshore wind park
[b]SM = submodule (of an MMC)

$R' = 6.825$ mΩ/km—for all three conductors. Specific cable parameters are comparable to [25] or [26]—and are just chosen as one example; the concept should be applicable to any kind of HVDC cable. The DC-HSSs at each line end are modelled as ideal switches with a maximum residual current interruption capability of 50 A.

3.2 | Implementation of decoupling sequence

To decouple the two point-to-point export links (either symmetrically or asymmetrically) once a decoupling sequence has been requested by the master control, the current flow via the interconnection cable(s) needs to be controlled to a value close to zero prior to opening the DC-HSSs. The decoupling sequence is depicted in Figure 6, and DC-HSSs to be opened are marked red. Depending on the load flow and wind power distribution at the time of the desired decoupling action, the current flow via the P, N, and DMR cables of the coupling line can differ. Whereas in some situations it could be close to zero without further actions, the worst case (in terms of the highest current on the coupling line) is a transfer of 500 MW via each pole of the coupling as shown in Figure 6, resulting in a current near 1 kA.

In order to allow decoupling under such conditions, the following steps are required (cf. also Figure 6, bottom) [14]:

1. Controlling the coupling line current(s) near to zero
2. Opening of the relevant DC-HSS(s)
3. Reconfiguration of DMR grounding (sym. decoupling)

To achieve a current close to zero on the relevant coupling line(s)—that is, for step 1—a controlled load flow change is to be implemented. In order to avoid wind power curtailment, the control sequence presented in this paper purely relies on changing the setpoints of the onshore converter stations. As the coupling line current cannot be measured directly at the onshore converters, an open-loop control (no feedback loop with measured coupling line current) is applied. More specifically, a (V_{DC}/P)-droop control—a comparatively simple and commonly used approach for MTDC voltage control as described in [27] and depicted exemplarily in Figure 6 (top left)—is implemented at all onshore stations; independent setpoints can be given for each P and N pole converter. The steady-state load flow settings before decoupling are given as (V_{DC}/P)-pairs for the onshore, and as a P-setpoint for the offshore converters.

To adjust the coupling line current flow as step 1, the droop characteristic—that is, the (V_{DC}/P)-setpoint—is shifted by the master controller as shown in Figure 6 (blue dotted lines) at all onshore stations—the droop constant itself is not changed. The onshore power setpoints P (indicated with p.u. numbers in ellipsoids in Figure 6) are set equal to the respective offshore wind power infeed, such that the coupling line current results close to zero. The V_{DC}-setpoints (given in Figure 6 in kV, converter output voltage pole-to-DMR) of all onshore converters are set according to a DC load flow calculation adapted to bipolar MTDC that is explained in Section 3.3.

For symmetrical decoupling, both P and N pole (V_{DC}/P)-setpoints are adjusted. For asymmetrical decoupling, the (V_{DC}/P)-setpoint is only changed for the pole to be decoupled via DC-HSS; however, the current flow and correlated voltage drop via the DMR have to be taken into account, requiring the V_{DC}-setpoint of the other pole to be adapted as well. For example, not only C1-P is changed from (523.05 kV | 0.5 p.u.) to (519.15 kV | 1 p.u.), but also the voltage setpoint of C1-N—although having a constant power setpoint—has to be changed from 523.05 to 525 kV. This effect is further described in Section 3.3.

Following the initialisation of the decoupling sequence, the DC-HSS opening (step 2) is triggered with a delay of 1 s. This time delay is chosen in order to allow the droop setpoint changes to become effective. The DC-HSS opening logic contains a current threshold, allowing the switches to be opened only when the current is below 50 A—see also discussion of switchgear speed in Section 4.3. After DC-HSS opening, the system remains interconnected for asymmetrical decoupling, such that only one DMR grounding point is required (and allowed). The sequence for symmetrical decoupling contains a third step (cf. step 3): Closing the DMR grounding switch on the second export link, as shown in Figure 6 (top right). It is to be discussed whether this step shall be conducted before or after DC-HSS opening—that is, whether there are two DMR groundings for a short time, or one system is floating for a short time. As symmetrical decoupling requires the DMR current to be zero, there is no significant difference expected in the results. Here, as an example, the DMR grounding is closed 400 ms before DC-HSS opening.

3.3 | Set point calculation for bipolar operation

The calculation of (V_{DC}/P)-setpoints uses the desired power setpoints *P(i)* that lead to a near zero current as an input. In addition, the topology, cable lengths, and specific resistance as in Section 3.1 are considered to populate the SxS-admittance (here, the number of stations is $S = 4$) matrix $\boldsymbol{Y}$. The V_{DC} setpoints (pole-to-DMR at the terminal) are then obtained via:

1. Load flow calculation via Newton–Raphson method (cf. methods in [28, 29]) independently for P and N pole (as for monopolar systems). $V_{DC,P}(i)$ and $V_{DC,N}(i)$ are obtained. Station C3 is defined as a slack node.
2. Calculation of DMR voltage shift for each line and each station/terminal via Equations (1) and (2). This calculation uses the DMR current flow resulting from the independent P and N pole load flow from step 1.
3. Correction of DC voltage setpoints for each station i according to DMR voltage drop from step 2. This is modelled as an additional voltage source—similar to modelling a galvanic cross-coupling.

To consider asymmetrical operating states with DMR current flow (e.g. Figure 6 bottom) in step 2, the DMR voltage shift $V_{DC,DMR}(i)$ at the neutral point of each station—that is resulting from asymmetrical load flow in step 1—is calculated via:

$$V_{DC,DMR}(i) = \sum_{p=1}^{P(i)} \sum_{k=1}^{K(p)} \frac{I_N(k,k+1) - I_P(k,k+1)}{\boldsymbol{Y}_{k,k+1}} \quad (1)$$

$$I_x(k,k+1) = \left(V_{DC,x}(k) - V_{DC,x}(k+1)\right) \cdot \boldsymbol{Y}_{k,k+1} \quad (2)$$

In (1) and (2), x is the pole variable (either P or N), $i \in [1 \ldots S]$ is the station index, *P(i)* is the number of all paths p from station i to the slack station, and *K(p)* is the number of stations $k \in [1 \ldots S]$ along a path p. In case a path element of path p (i.e. a line from k to $k+1$) is already part of the sum from a previous path $p-1$, it is skipped in the calculation.

It should be noted that the DMR voltage shift is calculated relative to the slack station (here: C3), and not necessarily to the station where the DMR is grounded. As there is only a single DMR grounding in the system (i.e. no ground return), the impact of grounding location is negligible for the load flow—and only relevant for the resulting pole-to-ground voltages.

Based on this calculation, step 3 adapts the voltage setpoint for station i according to the following two equations:

$$V_{DC,P,new}(i) = V_{DC,P}(i) - V_{DC,DMR}(i), \quad (3)$$

$$V_{DC,N,new}(i) = V_{DC,N}(i) + V_{DC,DMR}(i). \quad (4)$$

In case of balanced/symmetrical operation of both poles—that is, for symmetrical decoupling, steps 2 and 3 do not change. However, for non-zero DMR currents as needed for asymmetrical decoupling, there is a significant difference which needs to be considered in the (V_{DC}/P)-setpoints.

For the considered 4-terminal linear network, even a manual calculation via the principle given above is feasible. For a symmetrical transmission of 0.5 p.u. from C4-P to C2-P (cf. Figure 6, middle, top), and slack node C3, the C2 voltage setpoint is calculated (via step 1 only) to $V_{DC,P}(C2) = 523.05$ kV—and the DMR current is zero due to symmetry. For the asymmetrical case (cf. Figure 6, middle, bottom), however, the mismatch in power flow between P and N pole is 0.5 GW. Using Equations (1) and (3), the resulting DMR voltage shift and converter voltage set point for C2 are:

$$V_{DC,DMR}(C2) = R' \cdot l_{3-2} \cdot \left(I_{N,3-2} - I_{P,3-2}\right) \quad (5)$$

$$V_{DC,P,new}(C2) = V_{DC,P}(C2) + V_{DC,DMR}(C2) \quad (6)$$

With the simplification that the DC voltage is 525 kV in the entire network, the current difference can be set to 0.5 p.u. of 1.905 kA, such that $V_{DC,P,new}(C2)$ results to 525.33 kV.

For larger HVDC networks, the presented calculation approach enables to re-use existing MTDC load flow scripts designed for monopoles or symmetrical operation of bipoles. Other approaches could lead to similar results and might be even more generalisable, for example methods presented in [30].

4 | SIMULATION RESULTS AND DISCUSSION

In this section, simulation results with regard to the decoupling sequence, and the DC fault behaviour in the decoupled state, are presented and discussed. A focus is put on the validation of the load flow control and the residual current through the interconnection cables' DC-HSSs.

4.1 | Decoupling sequence: Load flow, DC currents, DC high speed switches

The behaviour is shown for both symmetrical (Figure 7) and asymmetrical (Figure 8) preventive decoupling. The sequences are initiated at $t = 0.1$ s via a change of the onshore station setpoints. The current measurements are highlighted with blue, green and brown arrows in Figure 6. In both cases, the relevant DC currents (all three for symmetrical, only P-pole for asymmetrical decoupling) can be controlled to values near zero (<50 A, cf. Figures 7 and 8 top) within approximately 0.5 to 1 s. The settling time depends on the exact control implementation. For example, the operator may foresee longer waiting times between sequence initialisation (setpoint change) and the triggering of the opening of the DC-HSSs—for example, in the range of several seconds up to 1 min.

In case of symmetrical decoupling, all six DC-HSSs (three at each line end) open one second after the initialisation, such that two independent point-to-point links result (Figure 7 bottom). Also, the DMR grounding is successfully re-configured as

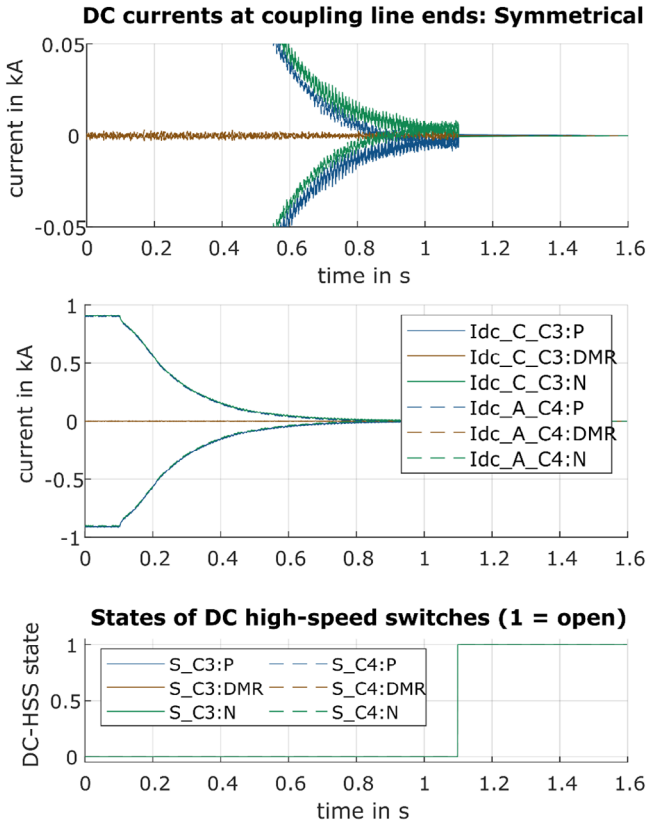

FIGURE 7 Symmetrical decoupling; top: DC currents on coupling line (with zoom-in); bottom: switching state of DC High-Speed Switches (DC-HSS) [14].

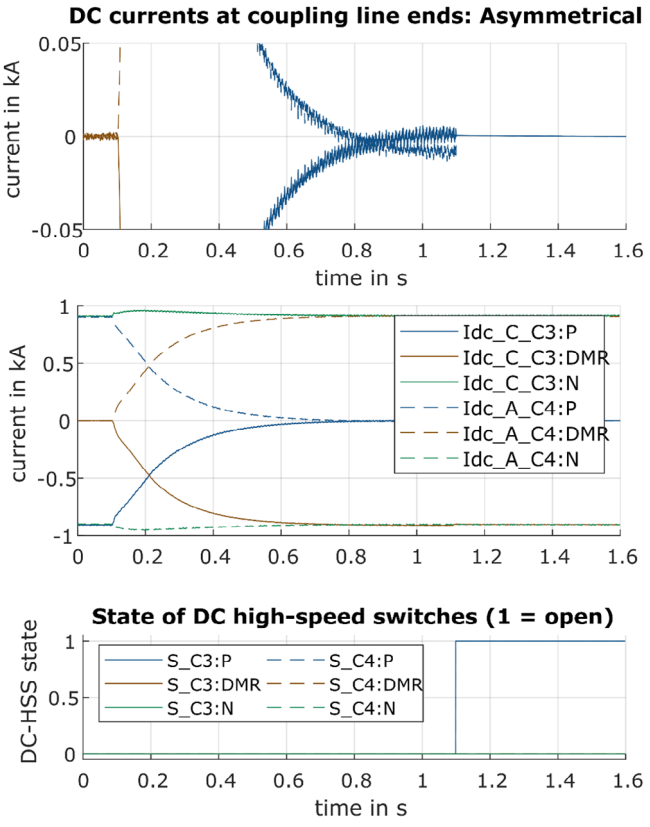

FIGURE 8 Asym. decoupling; top: DC currents on coupling line (with zoom-in); bottom: switching state of DC High-Speed Switches (DC-HSS).

described in Section 3.2 (not shown). In case of asymmetrical decoupling, the current is commutated from the P pole to the DMR due to the changed power setpoints (Figure 8). As visible from Figure 8 bottom, the DC-HSSs of the P pole open once the current has decayed to near zero, the other DC-HSSs stay closed.

The change in power flow for both the symmetrical and the asymmetrical decoupling cases is visualised in Figures 9 and 10 respectively. Here, the AC-side active power is shown for all $S = 4$ converter stations (top of figures, positive power indicates rectification), and the DC-side power is shown for both onshore converters for P and N poles (bottom of figures, positive power indicates inversion).

For symmetrical decoupling, it can be seen that all values reach the target values shown in Figure 6 (top, middle)—symmetrically on both P and N pole. For asymmetrical decoupling, the target values shown in Figure 6 (bottom, middle) are also reached: the active power transfer on the N pole (green curves) remains nearly unchanged, while the power on the P pole is changed.

4.2 | DC fault behaviour

In the following, the results of DC fault simulations are shown for the cases from Figure 2—as the main intention of the preventive DC-side decoupling is to limit the loss of power infeed in the event of such faults. To focus on DC-side effects and the power loss seen on the AC side, the onshore AC grids are modelled via Thévenin equivalents with a grid strength of 30 GVA (strong grid). For weaker grids or more detailed transmission grid models, effects on the AC voltage stability at the PoC—and also the impact of P-pole faults on the N-pole converter—should be studied to fully assess the system's integrity [31].

4.2.1 | Symmetrically decoupled system

For symmetrical decoupling (Figure 2, right), the DC fault behaviour is—by construction—identical to the behaviour of two separate point-to-point links. As there is no electrical connection between both links, no dedicated simulations are performed.

4.2.2 | Asymmetrically decoupled system

For asymmetrical decoupling (Figure 2, middle), the DC fault behaviour should be analysed as the system is still electrically coupled via DMR and one pole. In the following, both a pole-ground fault on the decoupled pole (Figure 11 top), as well as a pole-pole-ground fault (Figure 12 top, affecting both poles)

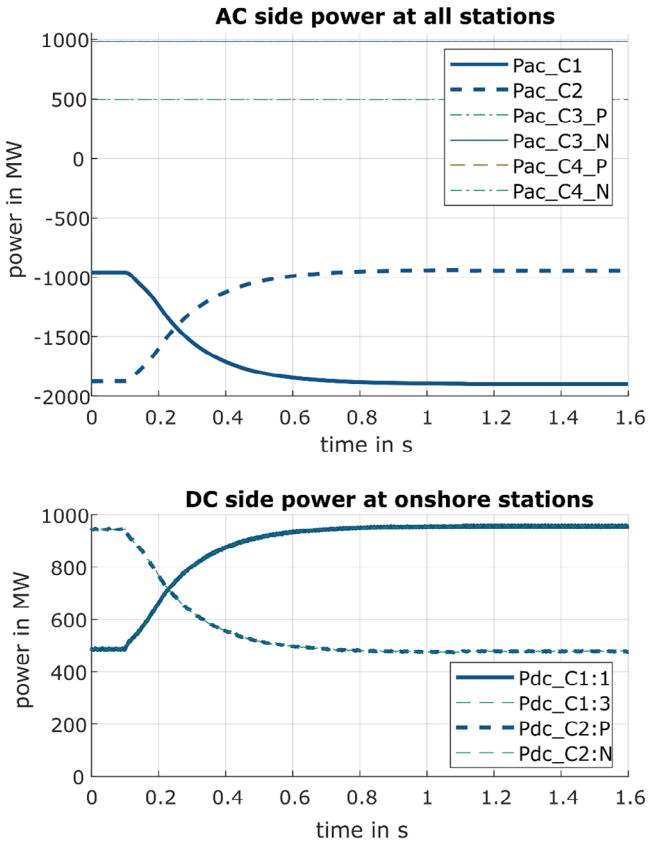

FIGURE 9 Sym. decoupling; AC- and DC-side power measured at onshore stations following a setpoint change at $t = 0.1$ s setpoints according to Figure 6 (left → top middle).

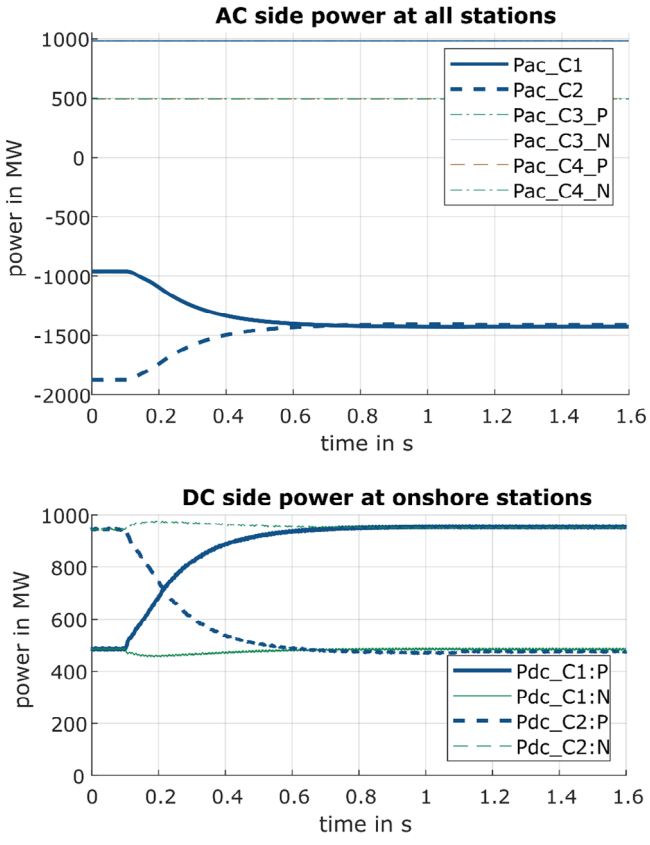

FIGURE 10 Asym. decoupling; AC- and DC-side power measured at onshore stations following a setpoint change at $t = 0.1$ s setpoints according to Figure 6 (left → bottom middle) [14].

are considered. Due to the system's symmetry, the results are transferable to the other link and/or the other pole. For all cases, a maximum wind infeed at rated power (4 GW) is assumed. The corresponding results are analysed to:

a. Validate that the power loss remains below 3 GW
b. Validate that the immediate post-fault states are stable.

In Figure 11, the DC voltages and currents for both onshore stations (C1 = bottom, and C2 = middle) are depicted. It can be observed that—as desired—the left HVDC link C1-C3 remains in operation, as well as the healthy pole of the faulted HVDC link C2-C4. Due to remote DMR grounding at C1, the potential at the neutral point of C2 is increased, and limited by a surge arrestor connected at the neutral point. Until DC fault clearing via ACCB opening at C2/C4, also the N-pole voltage at C2 is increased due to the DMR voltage shift.

For the pole-pole-ground fault, it can be seen from Figure 12 (bottom)—where both DC voltage and current are shown for station C2—that a transmission of 1 GW remains via the P pole. After fault clearing, the current flow continues via the positive pole and the DMR. As intended, the maximum temporary loss of power infeed does not exceed 3 GW. As for to the previous case, the DMR and healthy pole voltage at C2 shift temporarily, as the DMR grounding point is at the other end (C1) of the system. The DMR grounding could be re-configured to C2 by a secondary control action in order to operate the HVDC link C2-C4 fully independent.

For both fault cases, it has been shown that the preventive DC-side decoupling—even the asymmetrical option—successfully limits the impact of DC faults, such that at least one pole (1 GW) remains in operation, while all quantities remain within their tolerable limits during and after fault clearing.

4.2.3 | Coupled system: With and without DCCBs

In case the system is operated in a coupled manner without any DC circuit breakers, the entire faulted pole(s) will be affected and temporarily shut down (non-selective protection); the time-domain behaviour at both onshore converters is similar to the C2 behaviour shown in Figure 11. When the use of DCCB-based protection concepts (partially- or fully-selective as discussed in Section 2.2, shown in Figure 2 left) is desired, the fault behaviour strongly depends on the DCCB operating time, the size of current-limiting inductors, and the converters' overcurrent rating. A detailed analysis is not the focus of this paper, but has been done elsewhere [32, 33].

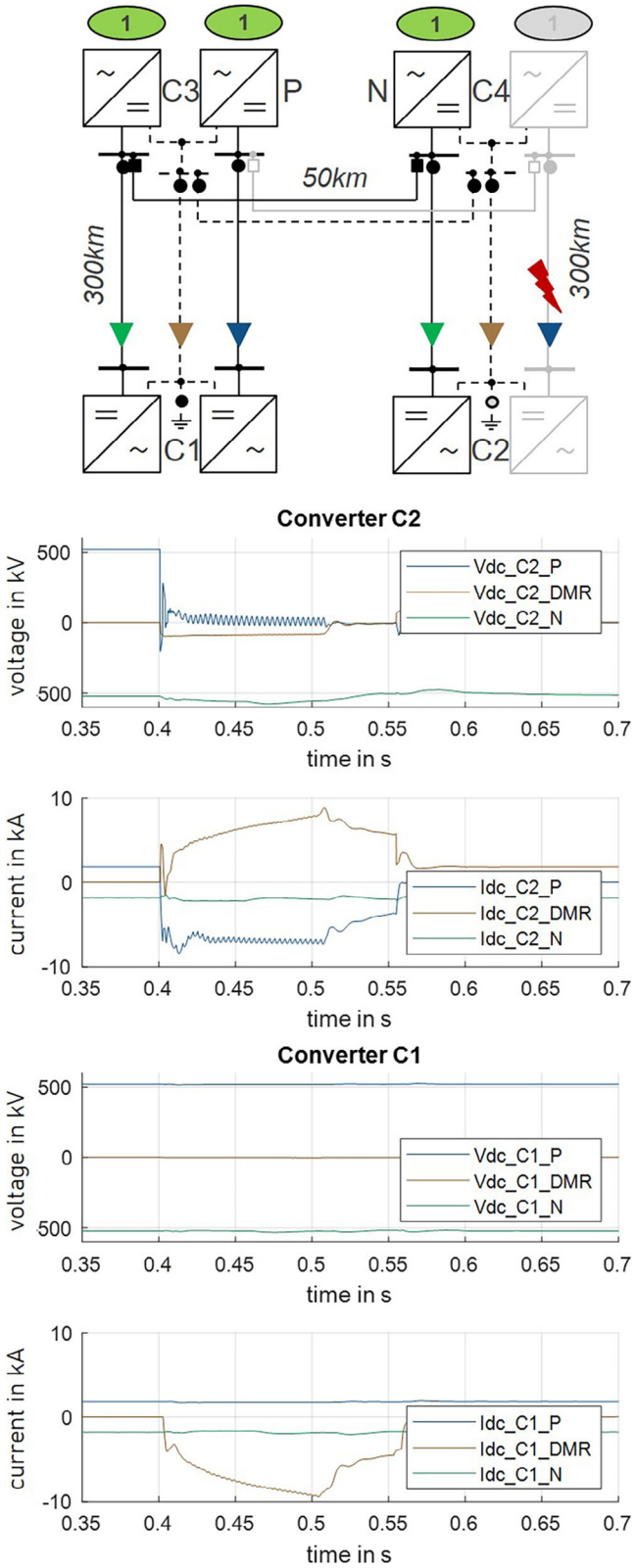

FIGURE 11 Pole-ground DC fault under asymmetrical decoupling: Overview (top) and DC-side measurements at C1/C2.

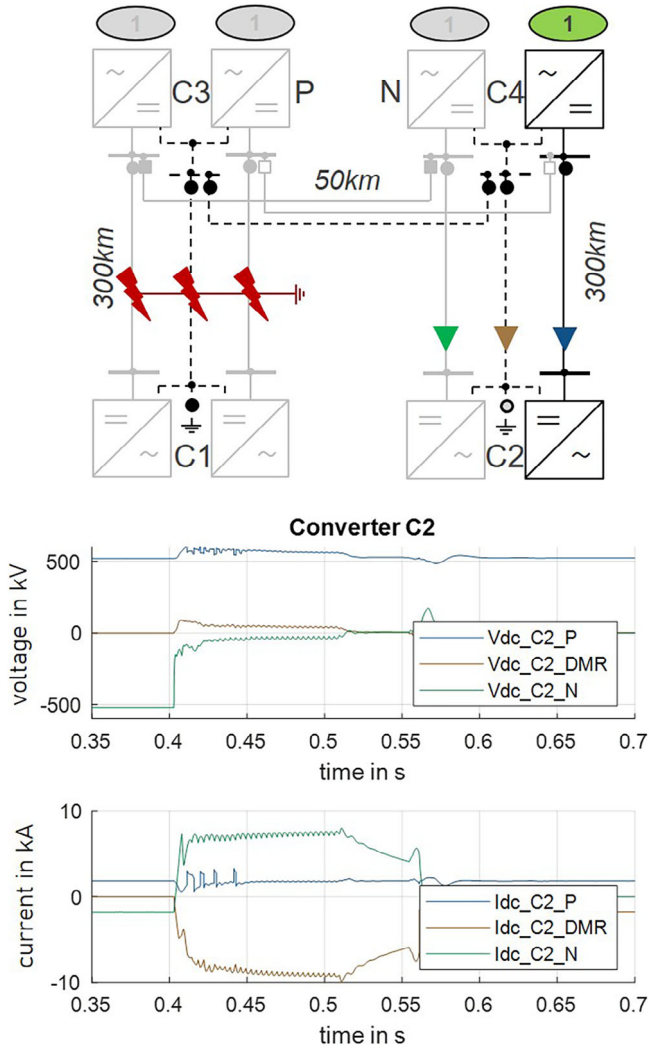

FIGURE 12 Pole-pole-ground DC fault under asymmetrical decoupling: Overview (top) and DC-side measurements at C2.

4.3 | Discussion: Challenges and limitations

Although it has been shown that (a) decoupling in normal operation is possible, and that (b) the impact of DC faults is successfully limited in the decoupled state, there are several challenges and limitations related to the proposed preventive DC-side decoupling strategy. These are analysed in the following. A focus is put on required supervisory controls, switchgear, as well as possible disturbances that have been simplified in the simulation study. Further, relevant aspects for an implementation of a coupling sequence (return to coupled operation as indicated in Figure 3) are discussed.

4.3.1 | System-level control architecture (AC/DC grid control)

To implement the decoupling sequence in a real system, a master / supervisory DC grid controller for the entire system

would be required as indicated in Figures 4 and 5. This controller requires at least access to the offshore wind park control (e.g., fix the wind turbines' setpoints and measure the active power), and to the dispatch control level of each HVDC converter station. It has to perform the setpoint calculation based on measurement data—which should be acquired as close as possible to the time of decoupling sequence initiation, but still has to respect sampling rates of the DC grid and dispatch controllers [14]. Further, the influence of the changed DC-side setpoints and the overall AC/DC system load flow needs to be assessed, and AC-side measures necessary to facilitate the load flow change may need to be coordinated in an AC/DC grid control.

4.3.2 | Coupling line current control under disturbances

Further, the proposed control sequence lacks a feedback loop, as the offshore DC current (i.e. the coupling line current) is not directly available at the onshore stations. Thus, the desired DC current value of near zero might not be reached in case there are disturbances in power infeed leading to deviations from the values assumed for the (V_{DC}/P)-setpoint calculation. Notably, due to the short offshore cable length (50 km), a voltage difference of 35 V already leads to a current of 100 A. Thus, the simple control approach chosen in this paper may be very sensitive against disturbances, measurement errors, and parametric uncertainties—and may require enhancements for a realisation in a project. Another important cause for disturbances to consider are wind gusts leading to transient peaks in the wind turbines' power output. Consequently, the wind power infeed might not be an ideal constant over the relevant time period of one or several seconds. Therefore, if a wind gust hits the offshore wind farms during the preventive decoupling sequence, deviations from the DC current depicted in Figure 7 (top) are possible in such a way that the threshold of 50 A is exceeded. In this case, the local protection of the HSS would have to prevent the HSS from opening resulting in uncertain delays for the decoupling.

To address this issue for a real application, the fixed DC-HSS opening delay that is implemented in this paper for simplicity should be replaced by a logic (e.g. in a supervisory control, or in the switchyard control) that tracks the current through the DC-HSS and determines an optimal opening time instant. Another option could be using the offshore converters—which have direct access to measurements of the offshore platform with a negligible delay—to actively control the coupling line current with a feedback control similar to the fault current control presented in [23]. However, it has to be analysed in how far the converter control and the converter-internal energy buffer are suitable to allow such an implementation.

Regardless of the implementation, sufficient time should be planned for the decoupling sequence. For the short duration of the sequence, the steady-state setpoint of all wind turbines should remain constant. If necessary, for example, due to wind fluctuations and wind turbine dynamics, the decoupling sequence needs to be repeated with adapted (V_{DC}/P)-setpoints based on updated measurement data. To avoid long periods of wind power curtailment, decoupling decisions based on the wind forecast should be made some time (e.g. 15 min) ahead.

4.3.3 | Requirements on switchgear

To realise the DC-side decoupling concept, the requirements on the switchgear must be clearly defined. In particular, (a) the capability to interrupt a residual DC current and (b) the opening speed of the switches, will define both the costs, and the requirements on the control sequence's accuracy in controlling the line currents to zero. DC-HSS are preferred over standard DC disconnectors due to the aforementioned sensitivity of the switch currents to small voltage disturbances at the offshore converters: Once a current near zero is detected, the switches should open as fast as possible to reduce the risks of increasing currents during the opening process itself.

Here, the aforementioned control of periodic current zero crossings might reduce the stresses. Further, the effect of switchgear wear should be assessed, as switching actions—both for decoupling, and for coupling—may be required more frequently than for other operational purposes, e.g. topology changes due to maintenance.

4.3.4 | Coupling sequence implementation

As indicated in Figures 3 and 4, a re-connection of decoupled HVDC links is foreseen in case the wind infeed drops significantly below 3 GW for a sufficient period of time. Thus, a coupling sequence needs to be further analysed and would require the following exemplary steps:

1. Open the grounding switches of coupling lines (in case they have been closed after decoupling)
2. Close the DC-HSSs at one end of the coupling line(s)—potentially using pre-insertion resistors (PIRs)
3. Adapt the (V_{DC}/P)-setpoints in a way that the prospective coupling line current is (close to) zero
4. Close the DC-HSSs at the other end of the coupling line(s)
5. Reconfigure the DMR grounding for symmetrical decoupling (note: depending on the DMR grounding concept, step 5 could be done at a different stage)

Starting from a symmetrically decoupled state, it is to be decided whether the re-connection is done pole by pole (via the asymmetrically decoupled state), or for both poles at the same time. For step 3, the same load flow calculations as for the decoupling sequence—cf. Section 3.3—can be applied. In case the coupling line is energised to 525 kV, the setpoints chosen in Figure 6 (middle) would lead to a steady-state current flow of zero once the DC-HSSs would be closed.

The main challenge for the re-connection is step 2, that is, the energisation of the interconnection cable(s) during normal operation (Figure 13, right). In case the DC interconnection

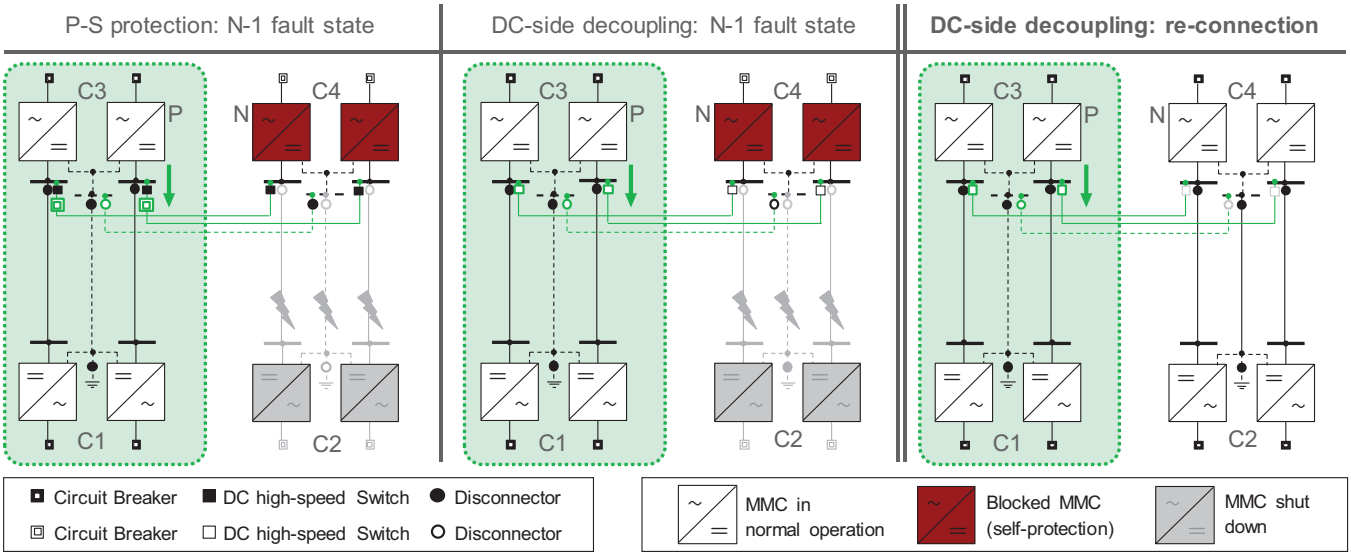

FIGURE 13 Re-connection via closing of switches for three different cases (from left to right): N-1 fault state for partially selective protection, N-1 fault state for symmetrical DC-side decoupling, and coupling sequence for symmetrical DC-side decoupling.

cable is grounded during the decoupled system operation, there will be transient charging currents once the DC-HSSs are closed on one end. These have to be limited in order to keep the HVDC link (marked with green-dotted area in Figure 13, here link C1–C3) in normal operation and to avoid tripping of any protection functions. It should be studied whether pre-insertion resistors are required in the DC switchyard, and how these are to be sized. However, this challenge is not unique to the aforementioned re-connection, and thus has not explicitly been modelled in the scope of the EMT study. It is required for planned topology changes in MTDC networks, and also for the post-fault reconfiguration when using a) preventive decoupling as presented in this paper (visualised in Figure 13 middle), or b) partially selective protection (visualised in Figure 13 right). For all cases depicted, it is required to energise a cable originating from an operational HVDC link.

5 | EXPANDABILITY CONSIDERATIONS

For the linear 4-terminal network (DC-side interconnection of two offshore HVDC links) under study, the proposed DC-side preventive decoupling strategy is shown to be an alternative to DCCB-based protection. In the following, the applicability to other small MTDC architectures is discussed, as well as the concept's expandability to larger linear MTDC networks.

5.1 | Application to other HVDC system architectures

First of all, the presented method is also applicable to monopolar HVDC networks—where only the symmetrical decoupling option exists. Compared to the cases shown in this paper, the complexity is lower, and no DMR reconfiguration is required. However, depending on their rating (e.g. 1 GW per station), the concept might not be required to interconnect two monopolar systems, as the maximum power loss is sufficiently low either way.

Considering recent plans for the North Sea, first 4-terminal MTDC networks will probably be bipolar systems, but they are not necessarily build in a Π-shape. They could also be realised as an offshore or onshore DC hub—in which two bipolar HVDC links are connected via a DC switchyard without any geographical distance [3, 34, 35]. Depending on the exact realisations, these topologies can be either radial or linear. The decoupling concept is also applicable to those radial or linear systems—and the realisation might be simpler, as there is no interconnection cable: There is only a single set of DC-HSSs to be switched, not two sets at opposite line ends—so less communication that is required. Further, there are fewer challenges for re-coupling, as these are mainly related to cable energisation, cf. Section 4.3.

5.2 | Expansion to larger networks

In general, the concept is also extendable to larger linear MTDC networks connecting $N > 2$ offshore HVDC links. The power flow control presented in Section 3.3 is applicable to any kind of bipolar linear MTDC network, such that the decoupling sequence can be realised in an analogous manner.

Depending on the AC-side constraints, and depending on the wind power infeed, larger systems could be decoupled into two or more separate subsystems—or remain coupled via a single pole only (asymmetrical decoupling). In the following, for simplicity, only the symmetrical decoupling option is discussed in more detail; also, any types of double busbars or other busbar configurations are not considered here. For a system expansion to $N = 3$ (6-terminal, feeding the same AC grid), two different symmetrical decoupling states exist:

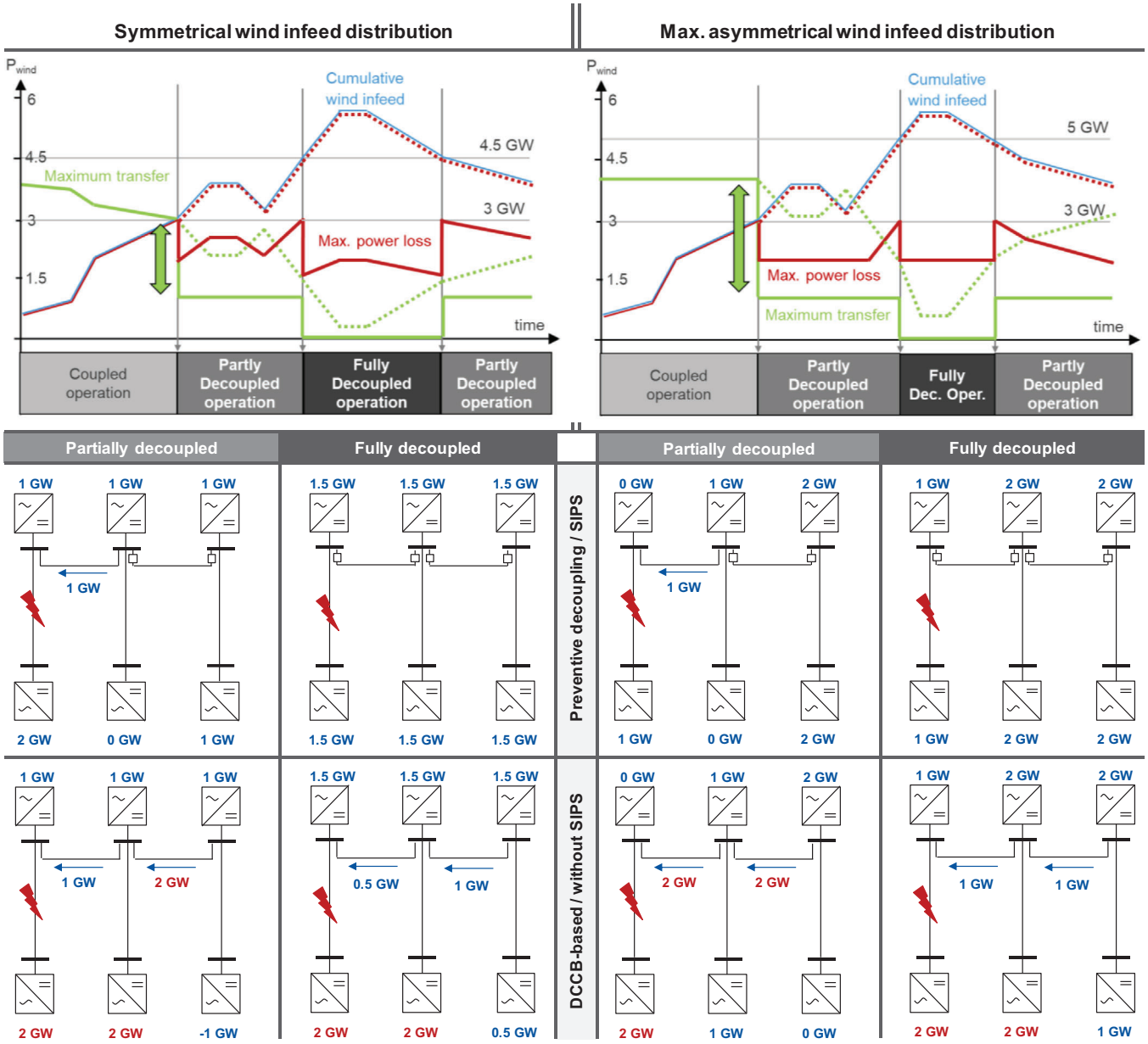

FIGURE 14 Symmetrical decoupling for $N = 3$ connected HVDC links. Top: Example timeline of cumulative wind infeed (blue), onshore power loss in case of a pole-pole-ground (P-P-G) fault (red), and maximum power transfer via coupling lines (green); Middle(decoupling)/bottom (DCCB-based): Single line diagrams for symmetrical (left) and asymmetrical wind infeed distribution (right).

a. Partly decoupled operation
b. Fully decoupled operation

These states, and their activation depending on the wind infeed, are visualised in Figure 14. At the top of the figure, the curves for wind infeed, power loss, and power transfer are shown analogously to Figure 6. At the bottom, simplified system diagrams (bipoles as a single line—symmetrical operation of poles assumed) including load flow are shown for the boundary conditions at which the decoupling to state (a) or (b) is activated. Two different distributions of the wind infeed are compared: Symmetrical (left) and maximally asymmetrical (right). For each, the red-marked "2 GW" indicates which components limit the power transfer in the fully coupled state ("without SIPS").

Whenever the cumulative infeed exceeds 3 GW, the system is decoupled at a single location (partial decoupling, state (a)). To select the decoupling location, it is proposed that the coupling line with the largest sum of its two adjacent offshore stations is chosen (cf. Figure 14 right, middle). Once the sum of infeed in one of the two subsystems of state (a) would exceed 3 GW again, the corresponding interconnection is decoupled, and the system is completely decoupled into its three point-to-point links. Notably, for $N > 2$, the boundary cumulative wind infeed at which the full decoupling (state (b)) is initiated depends on the distribution of the wind infeed, and varies between

4.5 GW (symmetrical) and 5 GW (max. asymmetrical). For larger networks, the difference will grow further.

Compared to a 4-terminal system, where decoupling only affects a cumulative wind infeed of >75% (i.e. approximately 2500 h/year) and a maximum of 1 GW transfer power flow (cf. Figure 6), the operational drawbacks are significantly higher for a 6-terminal system. The highest restriction of power transfer already occurs at the first decoupling action—that is, the transition to state (a). Already at a cumulative wind infeed of 50%, which is exceeded in ca. 3700 h/year [24], the power transfer is reduced by up to 3 GW (cf. Figure 14 top) compared to a coupled operation (e.g. with DCCBs used for protection).

Thus, for larger HVDC networks ($N > 2$), the costs of operational disadvantages might exceed the savings due to reduced protection equipment and lower complexity. As for the 4-terminal network, more detailed market and grid operation studies would be required for a full assessment, and the outcome will depend on the location of the HVDC links in one or multiple AC grids. For systems feeding different AC grids, the decoupling strategy could be limited by market restrictions. Further, for ring or meshed MTDC systems (e.g. created by adding an additional line to the linear 4-terminal network), an application of the preventive DC-side decoupling is not considered beneficial due to the reduced flexibility—and also the increased complexity of decoupling itself.

Overall, with increasing system size and/or the degree of meshing, the advantages of DCCB-based protection grow rapidly. DC-side decoupling could still be used as a back-up in case protection components have shown malfunctions and need to be replaced.

6 | CONCLUSION AND OUTLOOK

The preventive DC-side decoupling method proposed in this paper enables multi-terminal operation of offshore HVDC networks without the need for additional protection hardware—that is, without dependency on DC circuit breakers. It can be interpreted as an operational concept or a system integrity protection scheme (SIPS). As such, it may simplify and accelerate the first linear offshore DC-side interconnections—which are highly desired, but still considered a major challenge both from a technical as well as from a planning perspective.

The concept addresses the challenge that without a reliably working protection concept, DC faults might lead to power losses endangering the stability of connected AC grids. In contrast to the majority of DC-side protection approaches, this method is based on state-of-the-art technology: DC high-speed switches on the DC interconnection are preventively opened when the total amount of wind power exceeds the maximum tolerable power loss (e.g. 3 GW)—either on one or both poles. EMT simulations have shown the technical feasibility of both the de-coupling during normal operation, and the desired limitation of the power loss under faults in decoupled state.

As the proposed preventive DC-side decoupling method limits the impact of DC faults without the use of DC circuit breakers, it can partially avoid crucial interdependencies between control and protection interoperability—which are especially relevant in a multi-vendor context [11]. The solution is rather based on preventive operational management instead of the use of advanced technologies that require more complex specifications. This way, a first multi-terminal HVDC network in Europe might be realisable with a more conservative approach, a reduced need for interfaces and functional requirements, and thus within a shorter time frame.

As the concept leads to a limited power flow flexibility in decoupled state, further research is needed to evaluate its scalability to other MT-HVDC topologies and/or larger HVDC grids. Whereas for smaller linear multi-terminal HVDC networks, the disadvantage of reduced flexibility is expected to be tolerable, it might outweigh the benefits for larger and/or meshed networks. For such projects, both grid-level and HVDC-level studies should be performed to assess the concept's feasibility case-specific for each project idea. It is likely that the concept is an interim solution until more advanced technologies have matured for use in more complex HVDC structures. These advanced technologies—in particular DC circuit breakers—could for example be tested first within "safe to fail" pilot projects in which the total loss of infeed cannot exceed 3 GW.

AUTHOR CONTRIBUTIONS

Patrick Düllmann: Conceptualization; formal analysis; investigation; methodology; software; visualization; writing—original draft; writing—review and editing. **Christopher Klein**: Conceptualization; software; writing—review and editing. **Pascal Winter**: Conceptualization; validation; writing—review and editing. **Hendrik Köhler**: Conceptualization; validation; writing—review and editing. **Michael Steglich**: Validation; writing—review and editing. **Jan Teuwsen**: Validation; writing—review and editing. **Willem Leterme**: Funding acquisition; supervision; writing—review and editing.

ACKNOWLEDGEMENTS

The paper is an extended version of a conference publication [14] at the IET ACDC 2023 conference and has been invited to this special issue of IET GTD.

CONFLICT OF INTEREST STATEMENT

The authors declare no conflicts of interest.

DATA AVAILABILITY STATEMENT

The data that support the findings of this study are available from the corresponding author upon reasonable request.

ORCID

Patrick Düllmann https://orcid.org/0000-0001-5773-8493
Christopher Klein https://orcid.org/0009-0001-5138-3334

REFERENCES

1. Bundesamt für Seeschifffahrt und Hydrologie: Entwurf Flächenentwicklungsplan 2023. (2023). https://www.bsh.de/DE/THEMEN/Offshore/Meeresfachplanung/Flaechenentwicklungsplan_2023/flaechenentwicklungsplan_2023_node. Accessed 2 July 2024

2. eurobar.org: Eurobar—connecting europe offshore. https://eurobar.org/. Accessed 11 Apr 2023
3. North Sea Wind Power Hub Programme: Towards the first hub-and-spoke project—concept paper 2021. https://northseawindpowerhub.eu/sites/northseawindpowerhub.eu/files/media/document/NSWPH_Concept%20Paper_05_2021_v2.pdf. Accessed 2 July 2024
4. InterOPERA: InterOPERA Objectives: Mutually Compatible HVDC Systems. https://interopera.eu/objectives/. Accessed 5 Jan 2024
5. Moore, J., et al.: Towards a deployment plan for a future European offshore grid: Cost-benefit analysis of topologies. CIGRE Session 48, Paris, France (2020)
6. Institut für Elektrische Anlagen und Netze, Digitalisierung und Energiewirtschaft (IAEW): Nationale und Internationale Offshore-Vernetzung (2023). https://www.netzentwicklungsplan.de/sites/default/files/2023-06/Studie_Offshore-Vernetzung_2023_1.pdf. Accessed 1 July 2024
7. PROMOTioN: Deliverable D12.4 - Final Deployment Plan. https://www.promotion-offshore.net/fileadmin/PDFs/D12.4_-_Final_Deployment_Plan_Distributed_Version.pdf. Accessed 2 July 2024
8. Düllmann, P., Brantl, C., Tünnerhoff, P., Ruffing, P., Moser, A.: European offshore grid: On protection system design for radial bipolar multi-terminal HVDC networks. CIGRE Session 2022, Paris, France, SC B4 (2022)
9. Alefragkis, A., Kabul, S.: Next generation offshore grid connection systems: TenneT's 2 GW standard. ELECTRA N°321 no. 321 (2022)
10. Protection and local control of HVDC-grids, Technical Brochure 739, CIGRE JWG B4/B5.59 (2019)
11. ENTSO-E, ENTSO-E Position on Offshore Development: Interoperability. https://eepublicdownloads.entsoe.eu/clean-documents/Publications/Position%20papers%20and%20reports/210125_Offshore%20Development_Interoperability.pdf. Accessed 27 Sep 2021
12. Düllmann, P., Brantl, C., Klein, C., Moser, A.: Interdependencies in HVDC grid protection: Impact of converter parameters and controls on DC fault-ride-through capabilities and protection system design. IET Gener. Transm. Distrib. 17(10), 2356–2375 (2023). https://doi.org/10.1049/gtd2.12812
13. Stanković, S., Hillberg, E., Ackeby, S.: System integrity protection schemes: Naming conventions and the need for standardization. Energies 15(11), 3920 (2022). https://doi.org/10.3390/en15113920
14. Düllmann, P., et al.: Preventive DC-side decoupling: A control and operation concept to limit the impact of DC faults in offshore multi-terminal HVDC systems. In: Proceedings of the 19th International Conference on AC and DC Power Transmission (ACDC 2023), pp. 30–37. IEEE, Piscataway, NJ (2023). https://doi.org/10.1049/icp.2023.1304
15. Plet, C.A., Hoffmann, M., El-Khatib, W., Alefragkis, A., Kurrat, M.: Levelized energy cost improvement through concept selection and availability optimization for the Norfolk Windfarms' export links. CIGRE Session 48, Paris (2020)
16. Frequency Stability Evaluation Criteria for the Synchronous Zone of Continental Europe. ENTSO-E, Bruxelles, Belgium (2016)
17. Official Journal of the European Union: Commission Regulation (EU) 2017/1485 establishing a guideline on electricity transmission system operation. (2017)
18. Brantl, C., Knechtges, M., Düllmann, P., Meier, C., Moser, A.: Requirements on offshore HVDC grid protection: Interaction with AC system inertia and fast frequency support. Presented at the 41st Cigre Symposium, Ljubljana, Slovenia. 21–23 November 2021
19. Dave, J., Ergun, H., van Hertem, D.: Incorporating dc grid protection, frequency stability and reliability into offshore dc grid planning. IEEE Trans. Power Delivery 35(6), 2772–2781 (2020). https://doi.org/10.1109/TPWRD.2020.3011897
20. Wang, M., Leterme, W., Chaffey, G., Beerten, J., van Hertem, D.: Multi-vendor interoperability in HVDC grid protection: State-of-the-art and challenges ahead. IET Gener. Transm. Distrib. 15(15), 2153–2175 (2021). https://doi.org/10.1049/gtd2.12165
21. Tünnerhoff, P., Brantl, C., Ergin, D., Schettler, F., Schön, A., Döring, D.: Impact of the DC circuit breaker design on selective fault detection and clearing methods in multi-terminal HVDC systems. In: Proceedings of the 15th IET International Conference on AC and DC Power Transmission (ACDC 2019), pp. 1–6. IEEE, Piscataway, NJ (2019)
22. Jahn, I., Hohn, F., Sharifabadi, K., Wang, M., Chaffey, G., Norrga, S.: Requirements for open specifications in multivendor HVDC protection systems. In: Proceedings of the 15th IET International Conference on Developments in Power System Protection (DPSP 2020), pp. 1–6. IEEE, Piscataway, NJ (2020)
23. Ruffing, P.: HVDC Grid Protection Based on Fault Blocking Converters. IFHT, RWTH Aachen University, Aachen, Germany (2020)
24. Special Considerations for AC Collector Systems and Substations Associated with HVDC- Connected Wind Power Plants: Technical Brochure 612, CIGRE WG B3.36, Paris, (2015)
25. Tackenberg, V., Welsch, J., Stenzel, D.: InterOPERA D3.1: demonstrator definition & system design studies (2024). https://interopera.eu/publications/. Accessed 2 July 2024
26. Torwelle, P.: NSWPH MT HVDC Functional requirements: Background report step-by-step guide on functional requirements and parameter ranges definition for HVDC building blocks (2023). https://northseawindpowerhub.eu/files/media/document/NSWPH-MTDC-FR_4047-Report%20DB3%20Rev05.pdf. Accessed 15 May 2024
27. van Hertem, D., Gomis-Bellmunt, O., Liang, J., (eds.): HVDC Grids: For Offshore and Supergrid of the Future. IEEE Press, Piscataway NJ (2016)
28. Teixeira Pinto, R.: Multi-Terminal DC Networks: System Integration, Dynamics and Control. Ph.D. Thesis, TU Delft (2014)
29. Beerten, J., Cole, S., Belmans, R.: Generalized steady-state VSC MTDC model for sequential AC/DC power flow algorithms. IEEE Trans. Power Syst. 27(2), 821–829 (2012). https://doi.org/10.1109/TPWRS.2011.2177867
30. Jat, C.K., Dave, J., van Hertem, D., Ergun, H.: Unbalanced OPF Modelling for Mixed Monopolar and Bipolar HVDC Grid Configurations (2022). http://arxiv.org/pdf/2211.06283v1. Accessed 2 July 2024
31. Düllmann, P.: Bipolar VSC-HVDC: Impact of single-pole DC faults on healthy pole under weak AC network conditions: SC B4, PS1-2, Question 1.4. In: CIGRE 2022 Session: SC B4 Package (2022). https://www.e-cigre.org/publications/detail/session-2022-b4-session-2022-sc-b4-package.html. Accessed 2 July 2024
32. Düllmann, P., Deitert, M., Moser, A.: Offshore HVDC grids: Comparison and sensitivity analysis for fully and partially selective protection system design. Presented at the B4 International SC Meeting and Colloquium 2023, Vienna, Austria, 11–15 September 2023
33. Abedrabbo, M., Leterme, W., van Hertem, D.: Systematic approach to HVDC circuit breaker sizing. IEEE Trans. Power Delivery 35(1), 288–300 (2020). https://doi.org/10.1109/TPWRD.2019.2922253
34. Danish Energy Agency: Denmark's Energy Islands. https://ens.dk/en/our-responsibilities/offshore-wind-power/denmarks-energy-islands. Accessed 14 Dec 2023
35. TenneT TSO GmbH: Multiterminal Hubs. https://www.tennet.eu/de/projekte/multiterminal-hubs. Accessed 14 Dec 2023

How to cite this article: Düllmann, P., Klein, C., Winter, P., Köhler, H., Steglich, M., Teuwsen, J., Leterme, W.: Preventive DC-side decoupling: A system integrity protection scheme to limit the impact of DC faults in offshore multi-terminal HVDC systems. IET Gener. Transm. Distrib. 18, 3801–3816 (2024). https://doi.org/10.1049/gtd2.13214